ACADEMIC PRESS

Available online at www.sciencedirect.com
SCIENCE DIRECT®

Journal of Solid State Chemistry 173 (2003) 280–292

JOURNAL OF SOLID STATE CHEMISTRY

http://elsevier.com/locate/jssc

RE_3Ga_9Ge (RE = Y, Ce, Sm, Gd and Yb): compounds with an open three-dimensional polygallide framework synthesized from liquid gallium

Marina A. Zhuravleva and Mercouri G. Kanatzidis*

Department of Chemistry, Michigan State University, 320 Chemistry Bldg., East Lansing, MI 48824, USA

Received 1 October 2002; received in revised form 20 December 2002; accepted 27 December 2002

Abstract

The RE_3Ga_9Ge compounds (RE = Y, Ce, Sm, Gd and Yb) were synthesized at 850°C in quantitative yield from reactions containing excess liquid Ga. The orthorhombic crystal structure is characterized by a unique three-dimensional open Ga framework with parallel straight tunnels. In the tunnels, inserted are arrays of the RE atoms together with interpenetrated monoatomic RE–Ga–Ge planes. A complex *disordered* arrangement of the RE and Ga atoms is observed in the monoatomic plane. Depending on the extent of disorder, the crystal structure could be presented either in a sub-cell (no ordering) or in a super-cell (partial ordering). Single-crystal X-ray data for Ce_3Ga_9Ge sub-structure: space group *Immm*, $Z = 2$, cell parameters $a = 4.3400(12)$ Å; $b = 10.836(3)$ Å; and $c = 11.545(3)$ Å; super-structure: space group *Cmma*, $Z = 8$, cell parameters $a = 8.680(3)$ Å; $b = 23.090(7)$ Å; and $c = 10.836(3)$ Å. The refinement based on the full-matrix least squares on $F_o^2[I > 2\sigma(I)]$ converged to final residuals $R_1/wR_2 = 0.0226/0.0528$ and $0.0729/0.1569$ for the sub- and super-structures, respectively. The relationship between the disordered sub-structure and partially ordered super-structure is discussed. Magnetic susceptibility measurements show Curie–Weiss behavior at the temperatures above 30 K with the negative Weiss constants $\Theta = -49(1)$ and -7.7 K for Gd and Ce analogs, respectively. An antiferromagnetic transition is observed in the Gd analog at $T_N = 26.1$ K. The μ_{eff} obtained for both analogs is close to the RE^{3+} free-ion value.

Keywords: Intermettalic; Metallic flux; Gallium network; Superstructure

1. Introduction

In recent investigations aimed at developing new routes for the exploratory synthesis of intermetallics we have reported results in the quaternary systems RE/Ni/Ga/Tt (RE = rare earth; Tt = Si or Ge). We have described a number of new polygallides synthesized from reactions employing liquid Ga as the solvent. Examples include the tetragonal RE_2NiGa_{12} and $RE_2NiGa_{12-x}Si_x$ [1] with three-dimensional (3D) Ga framework, and the hexagonal $RE_{0.67}Ni_2Ga_{6-x}Ge_x$ [2] ($x < 1$) possessing a two-dimensional (2D) Ga structure. A Ga flux was also used by others in the synthesis of $RERu_2Ga_8$ [3] with 2D Ga-only sheets, and $RE_{1.34}Pt_4Ga_{10}$ [4], where Ga atoms form 2D As-type layers. Numerous ternary intermetallic polygallides with RE and transition metal such as RE_2NiGa_{10} [5] (RE = La, Ce), RE_3NiGa_{10} [6] (RE = Ce, Pr, Nd), $Ce_3Ni_2Ga_{15}$ [7], RE_4NiGa_{18} [8] (RE = Ce, Nd), $RE_2Ru_3Ga_{10}$ [3] and $RE_2Ru_3Ga_9$ [9] are also known. The variety of the geometrical configurations of Ga networks found in polygallides is both striking and unique, and the observed structures are fascinating. The diversity of the 2D Ga networks mentioned above includes square, pentagonal and triangular assemblies, as well as As-type puckered layers of Ga six-member rings. No apparent relationship exists between these phases and the much more studied Zintl phases [10]. This rich chemistry justifies a continued search for the new structure types. Our own efforts in the systems RE/M/Ga/Ge (M = transition metal) employing Ga flux were further extended to Co, Cu and Fe. Surprisingly, we found that particular reaction stoichiometries yield products of phase separation where the transition metal is excluded, and the major components of the reaction product are Ga-rich ternary rare-earth–gallide–germanides. In this work, we report the synthesis, crystal structure, and magnetic properties of the new family of compounds RE_3Ga_9Ge (RE = Y, Ce, Sm, Gd and Yb).

*Corresponding author. Fax: +1-517-353-1793.
E-mail address: kanatzid@cem.msu.edu (M.G. Kanatzidis).

0022-4596/03/$ - see front matter
doi:10.1016/S0022-4596(03)00057-4

2. Experimental section

2.1. Synthesis

Although members of this family were originally discovered in the reactions containing transition metals, the latter is not needed for their synthesis. The formation of the RE_3Ga_9Ge phase was observed for the RE = Y, Ce, Sm, Gd and Yb, whereas for the other RE such as La, Tb, Dy, Ho, Er and Tm this phase was not obtained. The reactions between the rare earth, Ga and Ge were carried out in the excess of molten Ga in alumina crucibles sealed in the evacuated ($<1\times10^{-4}$ Torr) silica ampules. The elements of typical purity 99.9% and higher (Cerac Inc.): RE (2.48 mmol), Ga (37.0 mmol), Ge (2.48 mmol) were mixed in the ratio[1] RE:Ga:Ge as 1:15:1 under a nitrogen atmosphere. The reaction mixtures were then slowly heated (60°/h) up to 1000°C, shortly (5 h) held at 1000°C to obtain proper melt, then cooled (75°/h) to 850°C and held there isothermally for 6 days and, finally, cooled at ~10°/h to ~200°C. The excess of Ga was removed in a two-step process: first by hot-temperature span-filtration forcing liquid Ga through specially designed filters by centrifuging at high speed (>3000 rpm) for approximately 30 s, and second by treating the product with ~3 M solution of I_2 in dimethylformamide (DMF) for 12–24 h. The product was subsequently rinsed with DMF, hot water, and dried with acetone and ether. No other products except the target phase RE_3Ga_9Ge (and recrystallized Ge) were observed. A quantitative yield of the phase was confirmed by powder X-ray diffraction (XRD) and the energy dispersive spectroscopy (EDS). The resultant crystalline product possessed needle to bar-like morphology and typical metallic luster. In some cases aggregation of needles into bundles was observed. The micrograph of a typical crystal of Sm_3Ga_9Ge is shown in Fig. 1.

2.2. EDS analysis and powder X-ray diffraction

Micrographs of the samples were taken with a scanning electron microscope (SEM) JEOL JSM-35C. A semi-quantitative elemental analysis by EDS was done on SEM equipped with NORAN Inc., EDS detector. The analysis was conducted at accelerating voltage 20 kV, and the collection count time was 30 s. The EDS analysis showed that the average elemental composition for all samples corresponded to "$RE_3Ga_{7.8}Ge_{1.6}$".

The X-ray powder diffraction (XRD) patterns were taken at room temperature on a Rigaku-Denki/Rw400F2 (rotaflex) rotating-anode (Cu$K\alpha$) powder diffractometer and a CPS 120 INEL X-ray diffractometer (Cu$K\alpha$) equipped with position-sensitive detector. Experimental powder patterns were compared to that calculated from single-crystal data using the CERIUS [2] software package [11].

[1] A larger than stoichiometric amount of Ge was used in order to compensate for the possible recrystallization of pure Ge from the molten Ga.

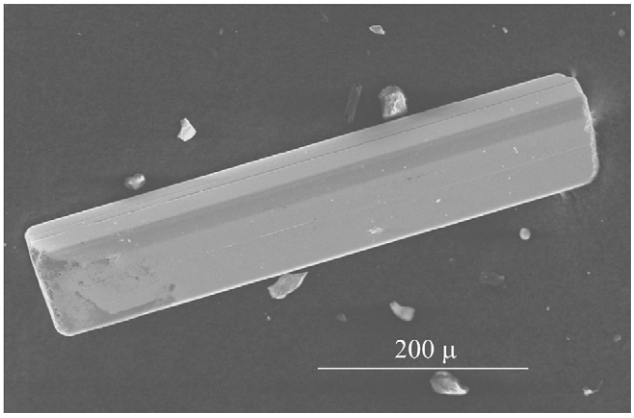

Fig. 1. SEM image of a typical RE_3Ga_9Ge crystal (RE = Sm).

2.3. Single-crystal X-ray crystallography

Single-crystal XRD data was collected on the Ce analog at room temperature with a Siemens Platform SMART CCD diffractometer. The needle-like crystal with the dimensions $0.12\times0.06\times0.05\,mm^3$ was mounted on glass fiber. A full sphere of reflections up to 76° in 2θ (Mo$K\alpha$ radiation, λ = 0.71073 Å, the X-ray radiation was generated at 34 kV/40 mA) was acquired using an exposure time of 90 s per frame. The data collection and acquisition was performed with the SMART [12] software package and the SAINTPLUS [13] program was used for data reduction. The analytical absorption corrections were done using a face-indexing routine, and an empirical correction for absorption based on symmetry equivalent reflections was subsequently applied with SADABS software package. The crystal structure was solved with direct methods using SHELXTL program.

Although the initial cell reduction readily gave the orthorhombic C-centered lattice with the parameters a = 8.680(3) Å, b = 23.090(7) Å, c = 10.836(3) Å, subsequent determination of the space group failed due to ambiguity of the limiting conditions, namely: $h\,k\,l$: $h+k=2n$, $0\,k\,l$: $k=2n$, $h\,0\,l$: $h=2n$; $h\,k\,0$: $h,k=2n$; $h\,0\,0$: $h=2n$; $0\,k\,0$: $k=2n$; $0\,0\,l$: $l=2n$. When carefully examined, however, it became evident that the reflections with somewhat stronger intensity obeyed the following limiting conditions:

$0\,k\,l$: $k=4n+2$ when $l=2n+1$

and $k=4n+4$ when $l=2n$,

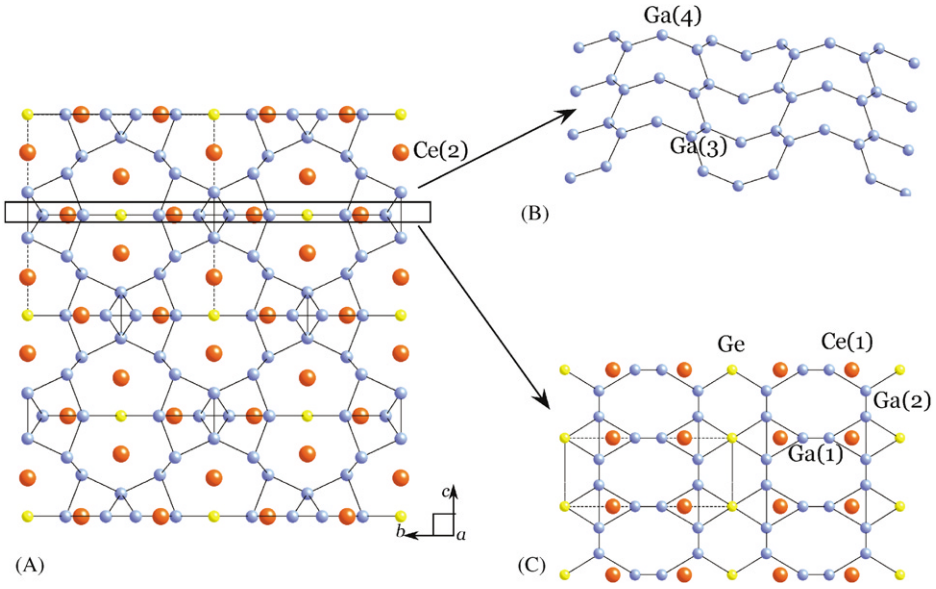

Fig. 2. (A) Projection of the sub-structure (*Immm*) of Ce_3Ga_9Ge onto *bc*-plane. Larger red spheres represent Ce atoms, smaller blue and light yellow spheres correspond to Ga and Ge atoms, respectively. For clarity, the bonds to Ce atoms are not drawn; (B) the Ga-only 2D puckered layer; (C) Fragment of the Ce–Ga–Ge plane viewed along the *c*-axis.

Table 1
Crystal data, (a) sub-structure and (b) superstructure refinement for Ce_3Ga_9Ge

Identification code	(a)	(b) $Ce_{2.93(1)}Ga_{8.66(2)}Ge_{1.02(3)}$
Formula weight	1120.43	1120.43
Temperature (K)	296(2)	296(2)
Wavelength (Å)	0.71073	0.71073
Crystal system	Orthorhombic	Orthorhombic
Space group	*Immm*	*Cmma*
Unit-cell dimensions (Å)	a =4.3400(12)	a =8.680(3)
	b =10.836(3)	b =23.090(7)
	c =11.545(3)	c =10.836(3)
Volume (Å^3)	542.9(3)	2171.8(11)
Z	2	8
d_{calc} (g/cm^3)	6.854	6.654
Absorption coefficient (mm^{-1})	36.866	35.788
Crystal size (mm^3)	0.2 × 0.06 × 0.05	0.2 × 0.06 × 0.05
θ range for data collection (deg)	2.58–29.19	2.58–29.19
Index ranges	$-5 \leqslant h \leqslant 5$	$-11 \leqslant h \leqslant 11$
	$-14 \leqslant k \leqslant 12$	$-31 \leqslant k \leqslant 26$
	$-15 \leqslant l \leqslant 13$	$-12 \leqslant l \leqslant 14$
Reflections collected	1769	6931
Independent reflections	429 [R_{int} = 0.0265]	1515 [R_{int} = 0.0449]
Refinement method	Full-matrix least squares on F^2	Full-matrix least squares on F^2
Data/parameters	429/33	1515/99
Goodness-of-fit on F^2	1.062	0.785
Final R indices [$I > 2\sigma(I)$][a]	R_1 = 0.0226, wR_2 =0.0528[b]	R_1 = 0.0729, wR_2 = 0.1569[c]
R indices (all data)	R_1 = 0.0247, wR_2 = 0.0536	R_1 = 0.1014, wR_2 = 0.1748
Extinction coefficient	0.00095(13)	0.00098(9)
Largest diff. peak and hole (e Å^{-3})	1.474 and −1.162	8.577 and −10.187

[a] $R_1 = \sum \|F_o|-|F_c\| / \sum |F_o|$; $wR_2 = [\sum w|F_o|-|F_c|^2 / \sum w|F_o|^2]^{1/2}$.
[b] $w = 1/[s^2(F_o^2) + (0.0301P)^2]$.
[c] $w = [1-\exp(-10s^2)]/[s^2(F_o^2) + (0.1235P)^2]$; where $s = \sin\theta/\lambda$ and $P = \mathrm{Max}(1/3F_o^2, 0) + 2/3F_c^2$.

$h\,0\,l$: $h = 4n + 2$ when $l = 2n + 1$
and $h = 4n + 4$ when $l = 2n$,

h k 0: h + k = 4n + 4.

Despite the unusual expression of the observed reflection conditions, they can be easily accounted for. The stronger reflections can be indexed if a sub-cell is assumed that is characterized with half a', b' parameters

(and therefore with doubled h', k' indices). This transformation ($a' = a/2$, $b' = b/2$, $c' = c$ or $h' = 2h$, $k' = 2k$, $l' = l$) leads to very clear conditions: $0\,k'\,l'$: $k' + l' = 2n$; $h'\,0\,l'$: $h' + l' = 2n$; $h'\,k'\,0$: $h' + k' = 2n$; $h'\,0\,0$: $h' = 2n$; $0\,k'\,0$: $k' = 2n$; $0\,0\,l'$: $l' = 2n$, that correspond to an I-centered cell $a = 4.3400(12)$ Å; $b = 10.836(3)$ Å and $c = 11.545(3)$ Å. This further leads to four possible space groups $I222$, $I2_12_12_1$, $Imm2$, and $Immm$, of which the highest symmetry space group $Immm$ was used for the sub-structure solution.

2.3.1. Sub-structure

A total of seven atomic positions were identified: the 4*g* and 4*j* for Ce atoms, 2*a* for Ge atom, and 4*g*, 4*i*, 8*l* and 8*n* were assigned to Ga atoms. Crystallographically it is very difficult to distinguish between the Ga and Ge atoms using X-ray data only due to the very small difference in their scattering. In this work, the differentiation between Ga and Ge was made on the basis of reasonable bond lengths and consistency with EDS elemental analysis, as done in previous work [14,15]. Because of the smaller covalent radius of Ge compare to Ga, the shorter Ce–*M* distances (where *M* could be Ga or Ge) were assigned to Ge. In previous investigations such assignments have proven correct by neutron crystallographic studies [16–18]. The resulting empirical formula Ce_3Ga_9Ge agreed well with the composition given by the EDS analysis. Further investigation of the Ga/Ge distribution should be done with methods able to distinguish between these elements, such as neutron diffraction or anomalous X-ray scattering with the use of synchrotron radiation.

see Fig. 2. Since such close proximity of the atoms does not represent a realistic picture, the occupancy parameters of the disorder atoms were freely refined. The resulting occupancies of disordered atoms varied between 0.49 and 0.51, and therefore in the final refinement cycle they were constrained to 1/2.

2.3.2. Super-structure

After achieving the sub-structure solution, we returned to the originally obtained larger *C*-centered cell, so that the observed super-structure reflections, although weak, could be taken into consideration. The ambiguity of the limiting conditions can be resolved by discarding the condition on either one of $h\,k\,0$ or $0\,0\,l$ set of reflections. Since the overall number of reflections satisfying the $h, k = 2n$ condition for the $h\,k\,0$ set was much larger than the $l = 2n$ in $0\,0\,l$ set, the latter was neglected. This yielded two possible space groups $Cm2a$ and $Cmma$, of which the centro-symmetric one was found to be more correct during the structure refinement. The group-subgroup relationship between sub-structure $Immm$ $(a'b', c')$ and super-structure $Cmma$ $(2a', 2c'b')$ goes through two subsequent *klassengleiche* transformations to minimal non-isomorphic subgroup of index 2: $Pmmm$ (a', b', c'), and $Cmma$ $(2a', 2c', b')$, the latter with a quadrupled cell volume

$$Immm - k2(a', b', c') \rightarrow Pmmm - k2(2a', 2c', b') \rightarrow Cmma.$$

In the super-structure, a total of 15 independent crystallographic atomic positions were refined; the correspondence of the sub-structure and super-structure atomic positions and their multiplicities combined with the occupancies (if partial) are given in the diagram below.

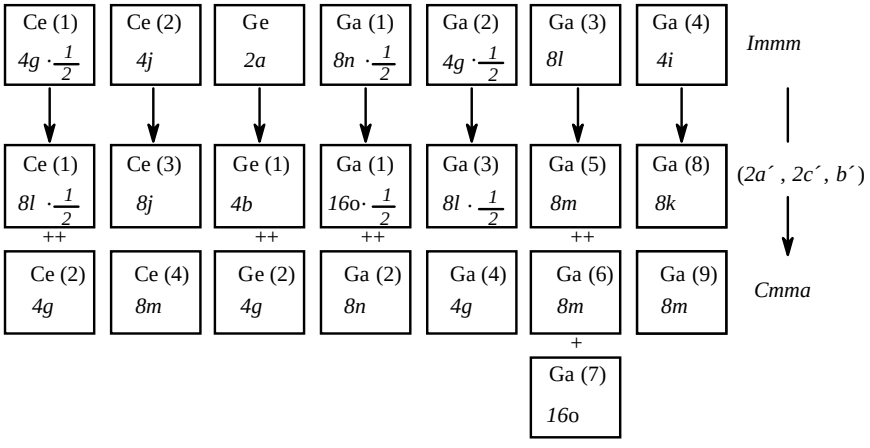

In the sub-structure, the Ce(1), Ga(1) and Ga(2) atoms form a monoatomic plane at $z = 0$; 1/2, where Ce–Ga and Ga–Ga are found at the distances as close as 1.452(2) and 1.629(3) Å from each other, respectively,

It is very important to note that the only difference between the super-structure with quadrupled cell and the sub-structure lies in the existence of two crystallographically distinct *RE*–Ga–Ge monoatomic planes.

Table 2
Atomic coordinates, equivalent isotropic displacement parameters ($Å^2 \times 10^3$) and occupancies for Ce_3Ga_9Ge (a) sub-structure and (b) super-structure

Atomic position	Wyckoff symbol	x	y	z	U_{eq}	Occ.
(a)						
Ce(1)	4*g*	0	0.2860(1)	0	9(1)	0.5
Ce(2)	4*j*	0	1/2	0.3101(1)	8(1)	1.0
Ge(1)	2*a*	0	0	0	9(1)	1.0
Ga(1)	8*n*	0.3123(3)	0.2041(1)	0	12(1)	0.5
Ga(2)	4*g*	0	0.4200(2)	0	15(1)	0.5
Ga(3)	8*l*	0	0.2100(1)	0.2937(1)	11(1)	1.0
Ga(4)	4*i*	0	0	0.3868(1)	11(1)	1.0
(b)						
Ce(1)	8*l*	1/4	0	0.2137(2)	16(1)	0.506(11)
Ce(2)	4*g*	0	1/4	0.2858(1)	6(1)	1
Ce(3)	8*j*	1/4	0.1551(1)	0	11(1)	0.960(12)
Ce(4)	8*m*	0	0.0950(1)	0.4998(1)	11(1)	0.960(12)
Ge(1)	4*b*	1/4	0	1/2	12(1)	1.01(2)
Ge(2)	4*g*	0	1/4	0.0003(2)	14(1)	1.02(3)
Ga(1)	16*o*	0.0943(4)	0.0025(1)	0.2957(3)	15(1)	0.464(11)
Ga(2)	8*n*	0.3442(2)	1/4	0.2036(2)	10(1)	0.972(13)
Ga(3)	8*l*	1/4	0	0.0802(5)	22(2)	0.487(18)
Ga(4)	4*g*	0	1/4	0.5802(2)	14(1)	0.971(18)
Ga(5)	8*m*	0	0.1054(1)	0.2094(2)	12(1)	0.959(15)
Ga(6)	8*m*	0	0.6006(1)	0.2108(2)	12(1)	0.956(15)
Ga(7)	16*o*	0.2554(1)	0.1470(1)	0.2898(2)	13(1)	0.962(13)
Ga(8)	8*k*	1/4	0.1935(1)	1/2	14(1)	0.976(19)
Ga(9)	8*m*	0	0.0566(1)	0.0011(1)	14(1)	0.975(18)

U_{eq} is defined as one-third of the trace of the orthogonalized U^{ij} tensor.

Thus, in the super-structure the planes located at $y = 0$, 1/2 are identical to the ones found in the sub-structure, i.e. disordered. On the contrary, the monoatomic planes at $y = \pm 1/4$ are perfectly ordered. Although the Fourier difference map shows the existence of high peak and hole (located at 0.11 and 1.44 Å from Ce(2) and Ga(4) atoms, respectively), this electron density cannot be accounted for by including it during the structure refinement. Thus, this high residual density is possibly a "Fourier noise" arising from the lack of sufficiently good data supporting the super-structure. The unconstrained refinement of the occupancy parameters of all atoms yielded the values of 0.956(15)–1.02(3) for the atomic positions of the ordered atoms, and 0.464(11), 0.487(18) and 0.506(11) for the disordered sites Ga(1), Ga(3) and Ce(1), respectively. These occupancy values were included in the final refinement. The positional parameters for both structures were standardized using the STRUCTURE TIDY [19] software. Details of the data collection and structure refinement for the sub- and super-structure solutions are listed in Table 1. The final atomic positions, equivalent thermal displacement parameters and occupancies for the sub- and super-structure are given in Table 2(a) and (b), respectively. The interatomic distances up to 3.5 Å are listed in Table 3(a) and (b) for sub- and super-cell, respectively. The complete crystallographic information has been deposited to the ICSD database.

2.4. Magnetic measurements

The magnetic susceptibility measurements were performed on a MPMS SQUID magnetometer (Quantum Design, Inc.) in the temperature range 2–350 K with an external applied magnetic field of 500 G. Polycrystalline samples of Ce_3Ga_9Ge and Gd_3Ga_9Ge were used for the isotropic measurements. A single-crystal sample of Gd_3Ga_9Ge was used to investigate the magnetic anisotropy with respect to the crystallographic axes. The crystals were positioned with the [100] crystallographic direction parallel and perpendicular to the external magnetic field. The data on field dependence of magnetization was collected for both analogs at 3 K for the fields up to ± 5 T.

3. Results and discussion

3.1. Reaction chemistry

The new ternary polygallides RE_3Ga_9Ge were isolated from the Ga-flux reactions containing *RE*, Cu, Ga and Ge (the ratio used was 4:1:30:4). From these reactions

Table 3
Bond lengths (Å) (a) sub-structure and (b) superstructure for Ce_3Ga_9Ge

Bond	Distance	Mult.	Bond	Distance	Mult.
(a)					
Ce(1)–Ga(2)	1.452(2)		Ga(1)–Ga(1)	1.629(3)	
Ce(1)–Ga(1)	1.6203(14)	× 2	Ga(1)–Ga(3)	2.6843(11)	× 2
Ce(1)–Ge(1)	3.0991(13)		Ga(1)–Ga(2)	2.704(2)	
Ce(1)–Ga(1)	3.1139(16)	× 2	Ga(1)–Ga(1)	2.711(3)	
Ce(1)–Ga(2)	3.185(2)		Ga(2)–Ga(2)	1.733(4)	
Ce(1)–Ga(3)	3.2228(8)	× 6	Ga(2)–Ga(4)	2.6772(9)	× 4
Ce(1)–Ga(4)	3.4342(9)	× 4	Ga(2)–Ga(1)	2.704(2)	× 2
Ce(2)–Ge(1)	3.0847(7)	× 2	Ga(3)–Ga(4)	2.5172(10)	× 2
Ce(2)–Ga(4)	3.1428(9)	× 2	Ga(3)–Ga(3)	2.5446(9)	× 2
Ce(2)–Ga(3)	3.1478(11)	× 2	Ga(3)–Ga(1)	2.6843(11)	× 2
Ce(2)–Ga(1)	3.2187(12)	× 4	Ga(4)–Ga(3)	2.5172(10)	× 2
Ce(2)–Ga(3)	3.3650(8)	× 4	Ga(4)–Ga(4)	2.614(2)	
Ge(1)–Ga(1)	2.5936(14)	× 4	Ga(4)–Ga(2)	2.6772(9)	× 4

(b) Bond	Distance	Mult.				Ga(1)–Ga(3)	2.699(6)	
Ce(1)–Ga(3)	1.447(6)		Ce(3)–Ga(7)	3.147(2)	× 2	Ga(1)–Ga(1)	2.705(7)	
Ce(1)–Ga(1)	1.619(4)	× 2	Ce(3)–Ga(2)	3.2158(16)	× 2	Ga(2)–Ga(7)	2.6688(19)	× 2
Ce(1)–Ge(1)	3.102(3)		Ce(3)–Ga(5)	3.3419(17)	× 2	Ga(2)–Ga(2)	2.704(3)	× 2
Ce(1)–Ga(1)	3.118(3)	× 2	Ce(3)–Ga(6)	3.3925(18)	× 2	Ga(2)–Ga(4)	2.705(3)	
Ce(1)–Ga(6)	3.1792(15)	× 2	Ce(4)–Ge(1)	3.0847(10)	× 2	Ga(3)–Ga(3)	1.738(10)	
Ce(1)–Ga(3)	3.185(5)		Ce(4)–Ga(6)	3.139(2)		Ga(3)–Ga(9)	2.674(2)	× 2
Ce(1)–Ga(5)	3.2618(16)	× 2	Ce(4)–Ga(8)	3.144(2)	× 2	Ga(3)–Ga(9)	2.681(2)	× 2
Ce(1)–Ga(9)	3.424(2)	× 2	Ce(4)–Ga(5)	3.156(2)		Ga(4)–Ga(8)	2.6770(15)	× 4
Ce(1)–Ga(9)	3.440(2)	× 2	Ce(4)–Ga(1)	3.180(3)	× 2	Ga(5)–Ga(9)	2.524(3)	
Ce(2)–Ge(2)	3.100(2)		Ce(4)–Ga(1)	3.262(3)	× 2	Ga(5)–Ga(7)	2.5680(16)	× 2
Ce(2)–Ga(2)	3.1178(19)	× 2	Ce(4)–Ga(7)	3.3396(18)	× 4	Ga(6)–Ga(9)	2.512(3)	
Ce(2)–Ga(4)	3.190(3)		Ge(1)–Ga(1)	2.594(3)	× 4	Ga(6)–Ga(7)	2.5278(16)	× 2
Ce(2)–Ga(7)	3.2510(15)	× 4	Ge(2)–Ga(2)	2.585(3)	× 2	Ga(7)–Ga(8)	2.518(2)	
Ce(2)–Ga(8)	3.4347(14)	× 4	Ga(1)–Ga(1)	1.637(7)		Ga(7)–Ga(6)	2.5278(16)	
Ce(3)–Ge(2)	3.0845(10)	× 2	Ga(1)–Ga(6)	2.680(3)		Ga(8)–Ga(8)	2.609(5)	
Ce(3)–Ga(9)	3.143(2)	× 2	Ga(1)–Ga(5)	2.683(3)		Ga(9)–Ga(9)	2.612(5)	

the Gd and Y analogs were initially obtained, along with binary $CuGa_2$ and Ge. Similarly, it was found that if the reaction involves Fe instead of Cu, the ternary polygallides are produced as a major phase, and the Fe is found in the binary compound $FeGa_3$. However, the RE_3Ga_9Ge phase was detected only in minor quantities if the reactions involved Ni or Co. The presence of Ni and Co favors the formation of quaternary compounds such as $RE_{0.67}Ni_2Ga_{5+n-x}Ge_x$ [2], $RENiGa_3Ge$ [18], $RE_3Ni_3Ga_8Ge_3$ [18], $RE_4Ni_3Ga_6Ge_4$ [20] and $RE_2NiGa_9Ge_2$ [21]. RE_3Ga_9Ge phases formed at low M:RE ratios ($\leqslant$1:4) and, of course, in the absence of the transition metal.

The large, well-formed single crystals of RE_3Ga_9Ge can grow easily in liquid Ga. The crystals adopt needle or bar-like crystal morphology, see Fig. 1. The aggregation of needles into bundles is found in some cases, and it is more common for the Ce analog or when short synthesis times were employed. The face-indexing procedure showed that the direction of the needle growth coincides with the [100] crystallographic axis, i.e. the crystal growth terminates quicker in the (bc)-plane but continues to propagate in the direction of the shorter a-axis.

The RE_3Ga_9Ge phases are very stable and form in a vide range of reaction conditions. For example, we have employed four different heating profiles seeking an improvement in the microscopic ordering in the crystal structures of the RE_3Ga_9Ge compounds. The temperature regimes with subsequently increasing time of isothermal step (6, 10 and 30 days) and, oppositely, with an extremely short (5 h) isothermal steps were carried out. For all RE elements we tried, the final product was pure RE_3Ga_9Ge phase, independent of the temperature profile. An exception was seen for Ce using the short profile, where a different ternary Ce/Ga/Ge phase [22][2] formed instead. Interestingly, neither the prolonged, nor shortened temperature profiles resulted in noticeably improved microcrystalline quality of the material.

[2] Composition as determined by EDS: $Ce_5Ga_{12}Ge_3$; cell parameters: a = 4.313(6) Å, c = 7. 419(7) Å, tetragonal.

Table 4
Room temperature cell parameters and volumes for RE_3Ga_9Ge (RE = Y, Sm, Gd, Yb)

Parameter	RE = Y	RE = Sm	RE = Gd	RE = Yb
a (Å)	8.396(2)	8.5390(18)	8.4420(12)	8.5037(18)
b (Å)	22.621(6)	22.770(5)	22.664(3)	23.007(4)
c (Å)	10.604(3)	10.695(2)	10.6337(15)	10.786(3)
V (Å^3)	2013.9(9)	2079.4(8)	2034.5(5)	2110.2(9)

The room temperature cell parameters and cell volumes for the isotypic compounds with RE = Y, Sm, Gd, Yb are shown in Table 4. The volume of the unit cell for Ce, Sm and Gd analogs indicates linear dependence with the atomic number of RE element, consistent with the lanthanide contraction. However, the anomaly is observed in cell volume of the Yb isotype, which is greatly increased compared to other analogs. This phenomenon is most likely associated with the presence of Yb in a Yb^{2+} oxidation state or mixed-valent Yb^{2+}/Yb^{3+} state.

3.2. Crystal structure

3.2.1. Sub-structure description

A projection of the RE_3Ga_9Ge sub-structure onto the bc plane is presented in Fig. 2a. The structure is three-dimensional, however, for the sake of simplicity it is worthwhile to sub-divide it into two 2D units: a monoatomic Ce–Ga–Ge plane and a Ga-only puckered layer. These 2D motifs alternate along the c-axis building a 3D structure, and the additional Ce(2) atoms are inserted in the remaining voids. Alternatively, the structure can be viewed as constructed of two independent interpenetrating sub-structures: an open 3D Ga-network (see Fig. 3) and Ce–Ga–Ge monoatomic planes. Ce(2) atoms fill in the remaining cavities.

The Ga-only puckered layer is depicted in Fig. 2b. In this layer, the Ga(3) and Ga(4) are arranged in the form of 8-membered rings in the boat conformation. The rings are condensed into a 2D puckered layer by sharing each of the eight sides with neighboring rings. The puckered layers extend in the direction perpendicular to the c-axis, and bind to each other through Ga(4)–Ga(4) interactions, thus forming a 3D Ga-only network with large tunnels running parallel to the a-axis. This Ga-only open framework unit is shown in Fig. 3. The shortest Ga–Ga distance in this structure (excluding the disordered atoms) occur in the 3D Ga-only framework; overall, Ga–Ga distances span the range from 2.5172(10) to 2.614(2) Å. These bonding contacts, thus, reflect rather strong Ga–Ga interactions, making the 3D Ga-only sub-structural unit a rigid polyatomic network. The observed distances are close to the sum of single-bonded metallic radii for Ga [23] (2.50 Å) and also comparable to those found in elemental Ga [24] (2.484–2.788 Å).

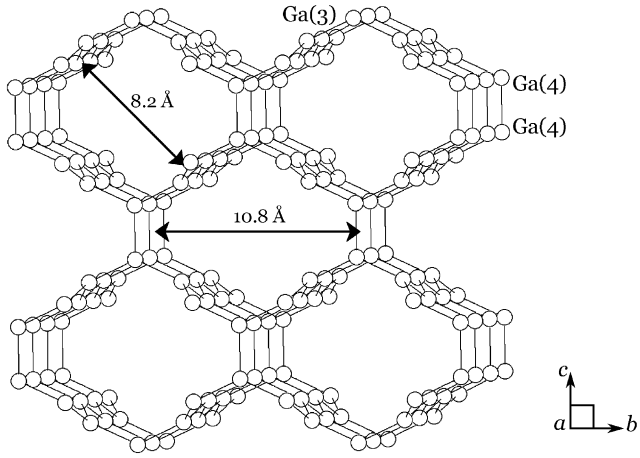

Fig. 3. The ordered Ga-only open 3D framework viewed along the a-axis ($Immm$). The Ga atoms represented in open circles. The bonds between the Ga atoms are drawn up to 2.62 Å. The tunnel openings (shown by arrows) measure ~ 11 Å in width and ~ 8 Å in height.

The fragment of the Ce–Ga–Ge plane, viewed along the c-axis, is shown in Fig. 2c. In this plane, the Ga atoms appear in a disordered arrangement forming a triangular mesh with unrealistic Ga–Ga bond distances (1.629(3) Å) between the triangles, while Ga–Ga bonds within the triangle are regular and close to 2.71 Å. The Ce(1) atoms fill in the center of the triangles additionally creating unreasonably short Ce–Ga bonds (1.452(2) and 1.6203(14) Å). A similar type of disorder between RE and Ga (or Al) was observed for $RENi_3Al_9$ [25], $RE_{0.67}Ni_2Ga_{5+n-x}Ge_x$ [2] ($n = 0, 1$), $RE_{1.34}Pt_4Ga_{10}$ [4] and $RE_4Pt_9Al_{24}$ [26]. As mentioned above, the occupancy parameter of each disordered atom refined to 50%, and this points to a simple ordering model. It is thus plausible to assume that the ordered arrangement is achieved when either the Ga_3 triangle is present and the Ce atom is removed from its center, or the Ce position is occupied while the Ga position comprising the triangle around it is vacant. This simple ordering scheme is shown in Fig. 4 (note that the cell parameters in the ordered plane have doubled along the a-axis).

The local coordination of Ce, Ga and Ge atoms is shown in Fig. 5. For clarity, only the ordered atoms are depicted. The Ce(1) and Ce(2) atoms have 14 and 12 neighbors within the distance of 3.5 Å, respectively. The coordination environment of Ce(1) includes thirteen Ga atoms with Ce(1)–Ga bonds ranging between 3.1139(16) and 3.4342(9) Å, and one Ge atom at 3.0991(13) Å. Similarly, Ce(2) has 10 Ga atoms bonded within 3.1428(9)–3.3650(8) Å, plus two Ge atoms connected at 3.0847(7) Å. Considering the sum of single-bonded metallic radii [23] of Ce (1.818 Å for CN = 12) and Ga (1.25 Å) these interactions could be regarded as weakly bonding. The Ce–Ga bond distances found in

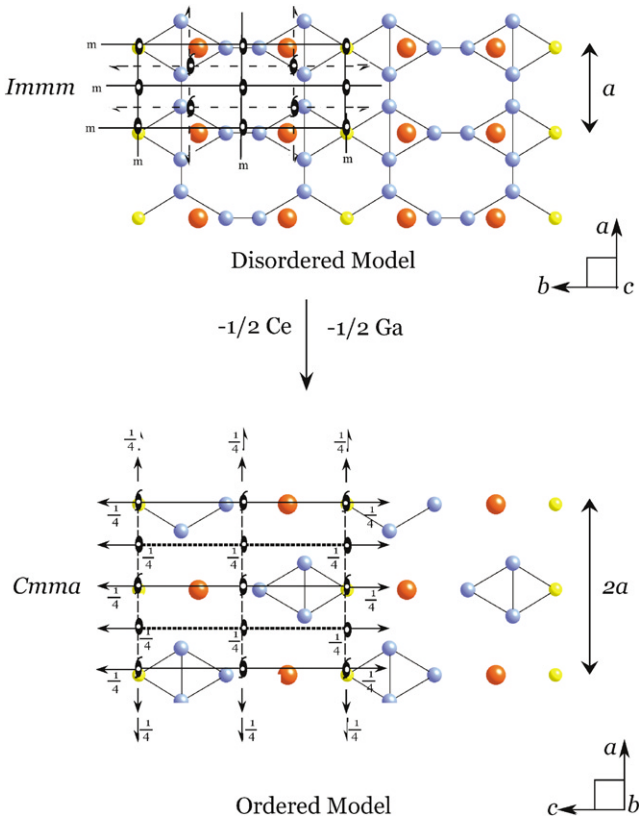

Fig. 4. Ordering scheme of the Ce, Ga, and Ge atoms in a selected monoatomic plane. An ordered arrangement (down) is achieved when half of Ce(1) and half of Ga(1) and Ga(2) atoms are removed from the disordered plane (up). The symmetry of the corresponding space group is superimposed onto the pattern of the plane to clarify the descent in symmetry in going from the sub-structure (*Immm*) to the super-structure (*Cmma*).

Ce_3Ga_9Ge are similar to those in $CeRu_2Ga_8$ [3], which cover the range from 3.135 to 3.387 Å. Note that the Ce–Ge distances are substantially shorter than the corresponding Ce–Ga bonds, in accordance with the original Ga/Ge assignment. Local coordination sphere of Ge atoms within 3.0 Å is comprised of four Ga(1) atoms that are located in-plane with Ge atom at 2.5936(14) Å. The Ga atoms within 3.0 Å adopt rather irregular coordination environments that include four to six other Ga atoms and a Ge atom, as shown in Fig. 5. The average distance found in Ce_3Ga_9Ge is 2.64 Å, quite shorter than the average Ga–Ga distance of 2.70 Å in metallic Ga [24]. This further reinforces the idea of strong covalent bonding within the Ga-only 3D network.

3.2.2. *Super-structure description: sub-structure–super-structure relationship*

Although the solution for fully ordered super-structure has not been obtained due to the lack of data, the intermediate super-structure solution exhibiting partially ordered arrangement was refined. This super-structure of Ce_3Ga_9Ge viewed along the *a*-axis is depicted in Fig. 6a, and it too could be thought as built of 2D units: a Ga-only puckered slab and a Ce–Ga–Ge monoatomic sheet. Again, the difference between the sub-structure and the super-structure lies in the packing and registry of the monoatomic layers along the *b*-axis. For example, in the super-structure the layers located at $y = 0, 1/2$ are identical to the ones found for the sub-structure and characterized by short distances between Ga(1), Ga(3) and Ce(1). The fragment of the disordered monoatomic layer at $y = 0, 1/2$ viewed along the *y*-axis is depicted in Fig. 6b. In contrast, the monoatomic planes situated at $y = \pm 1/4$ contain Ce(2), Ga(2) and Ga(4) that are arranged with regular interatomic distances. For example, in the $Ga(4)Ga(2)_2$ triangle the Ga–Ga distance is 2.705(3) Å, and the Ce(2)–Ga distance is 3.142 Å on average. This ordered type of plane is shown in Fig. 6c. Note that the ordered plane found in the super-structure and given in Fig. 6c is identical to the model shown in Fig. 4.

It is possible now to recognize the mechanism by which ordering of the Ce–Ga–Ge planes can take place by looking at the relationship between the sub- and the super-structure. It is evident from geometrical considerations that the disordered plane results from a superposition of two ordered planes shifted with respect to each other by the length of cell parameter a'. Fig. 7a illustrates a few unit cells of the disordered sub-structure ($Immm$, a', b', c') stacked along the c'-axis. If we were to glide every second unit cell along a' with respect to the one above and below, we would obtain a new structure shown in Fig. 7b. This super-structure is now defined by unit cell parameters that are $a = 2a'$, and $c = 2c'$. It is also clear that the lattice centering has changed from *I*-centered to *C*-centered.[3] Most importantly, the transformation results in ordering of half of the Ce–Ga–Ge planes. However, the other half of the planes that were located inside of the sub-cell (symmetry equivalent due to *I*-centering) have not changed and remained disordered. In Fig. 7 the ordered and the disordered planes of the super-cell are represented with the letters "O" and "D", respectively. The refined super-cell ($Cmma$, $2a', 2b', c'$) is given for comparison in Fig. 7c. It is evident that the proposed model for the super-structure has a full correspondence with the one refined from the XRD data. This is a *C*-centered four-fold super-cell with alternating ordered and disordered planes of Ce–Ga–Ge.

The presented model helps us to get an insight into the process that takes place during the crystal growth. Apparently, the crystal planes containing the monoatomic layer of *RE*–Ga–Ge can "slide" easily with respect

[3] The *b*- and *c*-axis were exchanged in going from the sub- to super-cell in order to conform to the standard orthorhombic setting.

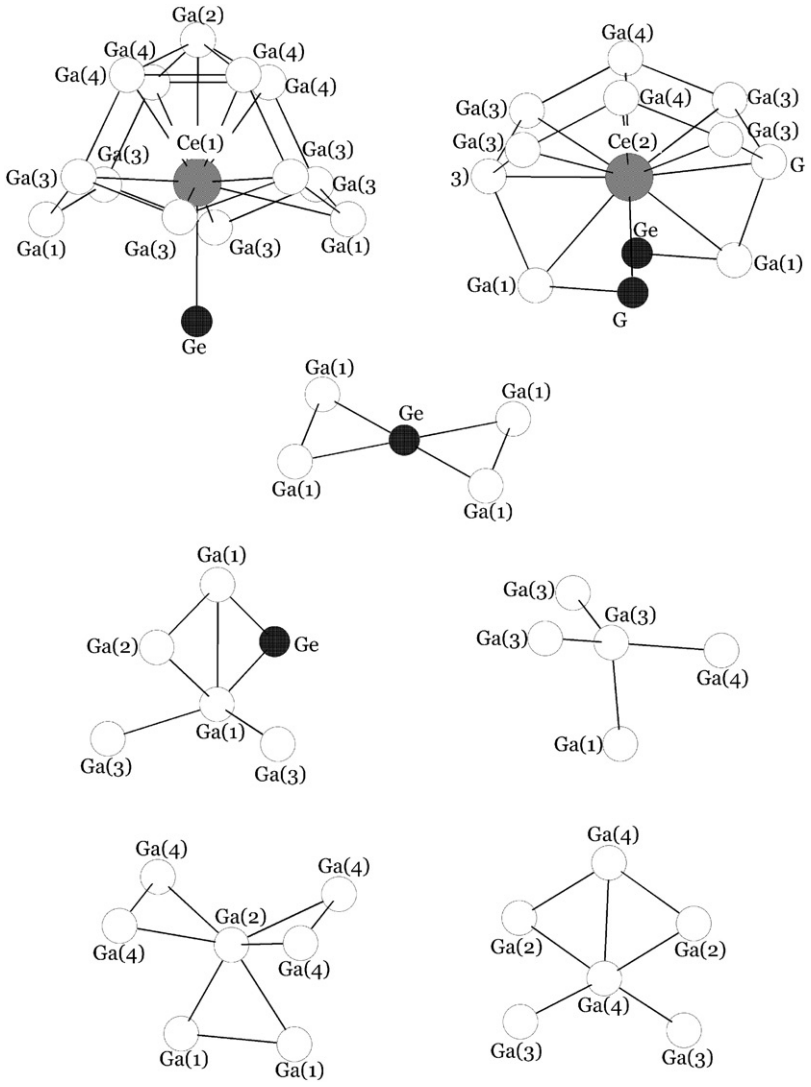

Fig. 5. Near-neighbor coordination environment of Ce atoms up to 3.5 Å and Ga, Ge atoms within 3.0 Å. Ga atoms are shown in open circles; larger and smaller filled circles represent Ce and Ge atoms, respectively.

to the rest of the structure. In other words, the energy barrier for this transformation seems to be comparable to the thermal energy, so that the process is activated at the temperatures at which the synthesis is carried out. Employing the different synthesis regimes with prolonged or shortened time we anticipated to obtain either the thermodynamic or the kinetic product that could possibly contain an ordered arrangement, where the planes are "locked" in place due to energy stabilization of given configuration. Unfortunately, a product with fully ordered planes was not obtained from these experiments.

It is also plausible to assume that an ordered arrangement could exist at the microscopic level, however, for a crystal of given size the stacking faults of the microscopic domains would produce both diffuse scattering and a statistical averaging of the X-ray data, and as a result a disordered picture. On the other hand, the completely opposite situation could hold true: in the absence of the short-range ordering of the planes, the infinitely large super-cell (up to a physical size of the crystal) would adequately describe the structure. Thus far, the data collected on a number of crystals with different rare-earth elements, crystal sizes, and different synthetic regimes did not lead to fully ordered structure solutions. Despite these indications, we searched for yet higher order super-structures looking at XRD axial photographs. The [$hk0$] and [$0kl$] zone photographs are presented in Figs. 8a and b, respectively. The photographs were taken on Y_3Ga_9Ge with an exposure time of 1480 and 800 s for the [$hk0$] and [$0kl$] zones, respectively. All the diffraction spots present in the pattern are well defined, leaving no indication for diffuse scattering. All present reflections could be indexed in the

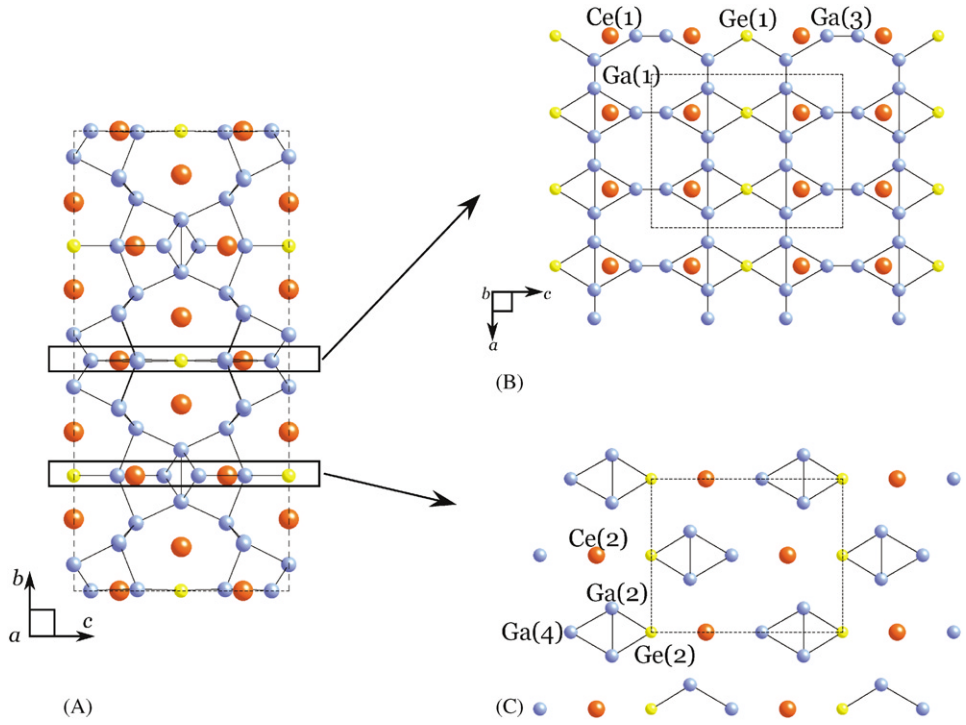

Fig. 6. (A) The super-structure of Ce_3Ga_9Ge projected on *bc* plane. The atoms are depicted in the same manner as for sub-structure. The excised monoatomic planes of (B) disordered and (C) ordered viewed along the *b*-axis.

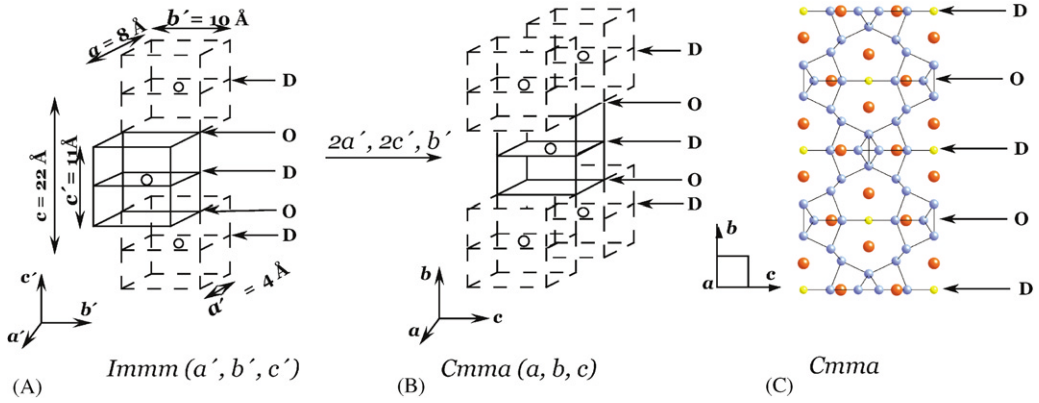

Fig. 7. (A–B) The transformation from the disordered sub-structure (*Immm, a′, b′, c′*) to the partially ordered super-structure (*Cmma,* $2a', 2c', b'$) via "sliding" of the sub-structure blocks by a'. (C) The refined super-structure (*Cmma,* $2a', 2c', b'$) is given for comparison. The ordered and disordered monoatomic planes are marked with letters "O" and "D", respectively.

super-cell ($2a'$, $2c'$, b'). No additional spots referring to a higher order super-cell were detected.[4]

[4] We emphasize that the collected intensity data that corresponds to the partially ordered super-structure was rather weak. The chance to obtain reliable X-ray data from an even higher order super-structure is thus greatly reduced. Perhaps, electron diffraction studies could provide more valuable information on the existence of the high-order super-cell due to stronger interaction of electrons with matter.

3.3. Magnetic properties

3.3.1. Gd-analog

The temperature dependence of the magnetic susceptibility and the inverse magnetic susceptibility of a single-crystal sample of Gd_3Ga_9Ge measured with the [100] crystallographic direction oriented parallel and perpendicular to the external field is presented in Fig. 9. In the high-temperature region (50–350 K) the reciprocal molar magnetic susceptibility (χ_m) obeys Curie–Weiss law. The extrapolation of the inverse susceptibility to

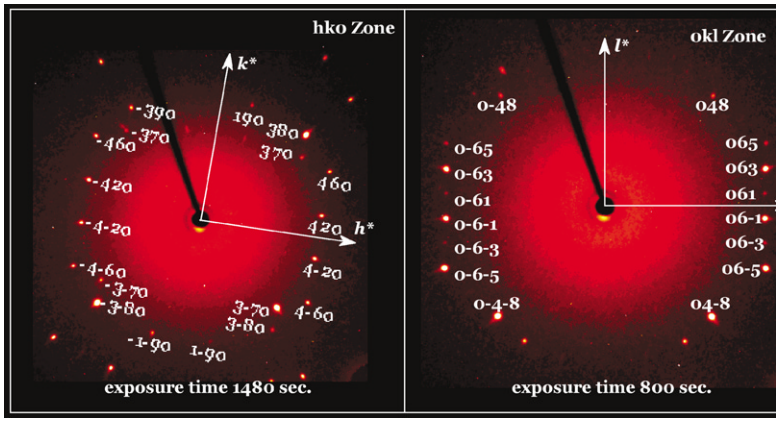

Fig. 8. (A) [$hk0$] and (B) [$0kl$] XRD zone photographs for Y_3Ga_9Ge. The Bragg spots are indexed in the $2a', 2c', b'$ super-cell.

zero yielded negative values of Weiss constants $\Theta_{||} = -48$ K and $\Theta_{\perp} = -50$ K. The effective magnetic moments $\mu_{\text{eff}}^{||} = 8.66$ BM and $\mu_{\text{eff}}^{\perp} = 9.0$ BM were obtained from the linear part of χ_{m}^{-1} vs. T, and appear to be rather high compare to the free-ion values[5] for Gd^{3+} (7.94 BM). Relatively large values of μ_{eff} were also observed for the $GdAl_{3-x}Ge_x$ [27] and Gd-containing equiatomic intermetallides [28,29]. An expanded region of χ_{m} at low temperatures is shown in the inset of Fig. 9. Below 30 K an onset of an antiferromagnetic ordering is observed. The broad maximum centered at ~15 K is seen in the case of $\chi_{\text{m}}^{\perp}$, but not in $\chi_{\text{m}}^{||}$, which continues to rise up to the lowest measured temperature of 2 K. Additionally, a minor variation in zero-field-cooled (ZFC)–field-cooled (FC) parts of $\chi_{\text{m}}^{||}$ was observed below 20 K, indicating weak history dependence. The isotropic data of magnetic susceptibility for Gd analog is consistent with the anisotropic measurements with a μ_{eff} of 8.39 BM and negative Weiss constant $\Theta = -49$ K.

In order to deduce the Néel temperature (T_{N}) of the antiferromagnetic transition for Gd_3Ga_9Ge, a set of isofield susceptibility measurements were done. The corresponding Néel temperature determined from the $\chi_{\text{m}} - \log T$ plots shown in Fig. 10 is 26.1 K. The field dependence of magnetization of the single-crystal and polycrystalline samples was measured in the fields up to 5 T. The saturation magnetization was not fully developed neither in isotropic, nor anisotropic type of measurements. The maximal value effective magnetic moment of only μ_{eff} ~4 BM was reached in the field of 5 T. Thus, the magnetic properties were found to be unaffected by the crystal orientation in both the temperature- and field-dependent susceptibility measurements. Similar results were obtained in the study of the quaternary $RE_{0.67}Ni_2Ga_{5-x}Ge_x$ [2] compounds of the late RE series (Sm, Gd–Tm), where the crystal field anisotropy was not expressed for the Gd analog solely. A negligible effect of the crystal field in these cases is connected to the properties of the S-ground state of the Gd^{3+} ion. It was shown [30] that in the absence of an angular momentum contribution to the total angular momentum the anisotropy effects due to crystal field vanish.

3.3.2. Ce analog

The temperature dependence of χ_{m} and χ_{m}^{-1} is given in Fig. 11a. The effective magnetic moment of 2.53 BM per Ce atom calculated from the linear part of the χ_m^{-1} vs. T plot is in very good agreement with the free-ion value for the Ce^{3+} ion (2.54 BM). The Weiss constant has small negative value of −7.7 K, indicating possible weak antiferromagnetic ordering. In the low-temperature region, see inset in Fig. 11a, the ZFC-FC part of susceptibility diverges at about 6 K, however continues to rise. Thus, up to 2 K no maximum in the χ_{m} vs. T plot was detected. The plot of the field dependence of magnetization is given in Fig. 11b. For the Ce analog, saturation magnetization is reached at about 1 BM, that is rather characteristic for Ce-containing ternary intermetallics [31–33] and is due to the effect of the crystal field splitting on $J = 5/2$ of the ground multiplet of Ce^{3+} atom [34,35]. This also is a possible cause of the slight non-linearity of the reciprocal magnetic susceptibility observed at higher temperatures.

4. Concluding remarks

The new ternary compounds RE_3Ga_9Ge (RE = Y, Ce, Sm, Gd and Yb) were obtained from reactions in molten Ga over a broad range of synthetic conditions. The crystal structure of RE_3Ga_9Ge consists of two interpenetrating sub-lattices: monoatomic RE–Ga–Ge planes and an open 3D Ga framework with large channels

[5] The effective magnetic moment of RE^{3+} free ion is given by the formula $g_J J(J+1)$, where J is total angular moment, and g_J is Landé factor.

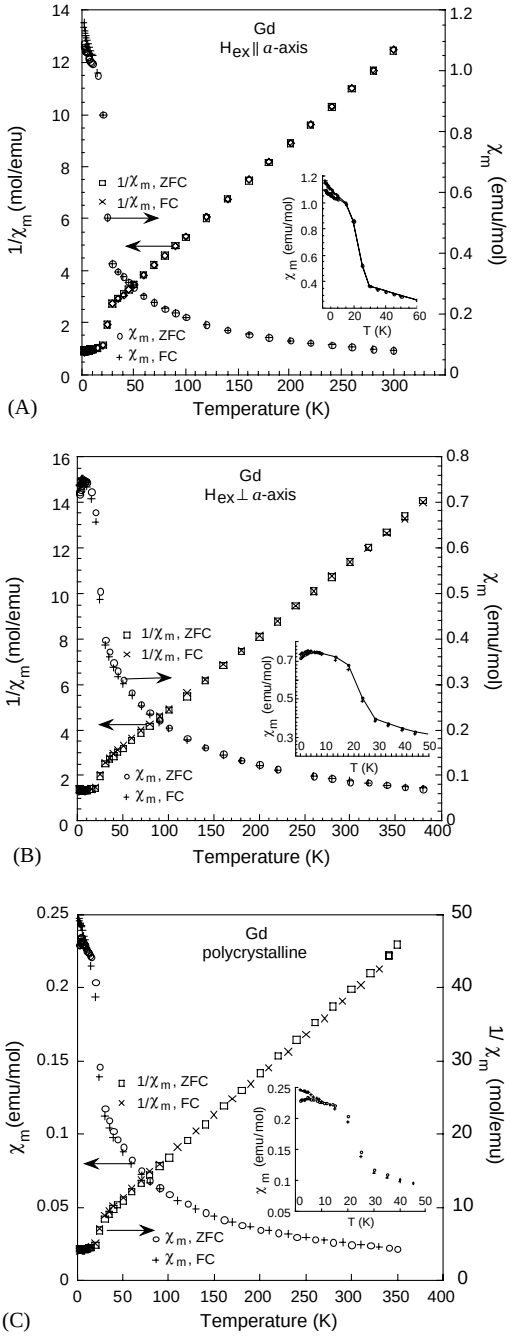

Fig. 9. Temperature dependence of molar magnetic susceptibility and inverse susceptibility of Gd_3Ga_9Ge single crystal oriented with [100] axis (A) parallel and (B) perpendicular to the external magnetic field (H_{ex}) and (C) susceptibility of the polycrystalline sample. The susceptibility is given per mole of Gd. Inset: temperature dependence of molar magnetic susceptibility and inverse susceptibility of Gd_3Ga_9Ge single crystal in the proximity of an antiferromagnetic transition temperature.

extending along the *a*-axis and filled with *RE* atoms. The Ga-only framework is a rigid structural unit held together via strong covalent Ga–Ga interactions with an average Ga–Ga bond distance being shorter than that in elemental Ga. Severe disorder exists between *RE* and Ga atoms in the monoatomic plane that is

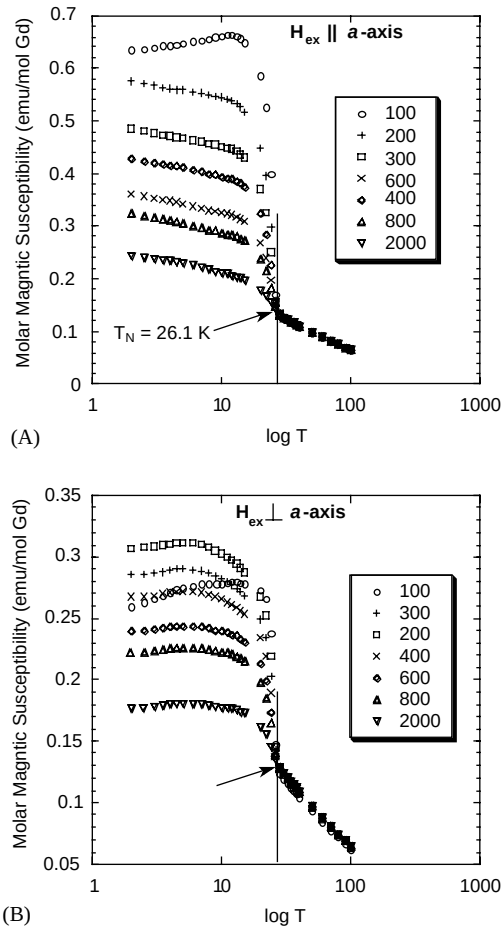

Fig. 10. Isofield plots of the molar magnetic susceptibility vs. temperature measured (A) parallel and (B) perpendicular to the external magnetic field. The applied fields were varied from 100 to 2000 G. The Néel temperature is the point at which the susceptibility measured at different fields diverges.

attributed to the unconstrained "sliding" of the planes during crystal growth. This sliding may reflect a relatively weak bonding between the two sub-lattices. On the basis of the investigation of the relationship between the sub- and the super-structure, a model for atomic ordering in the *RE*–Ga–Ge planes was proposed. The magnetic measurements performed on the Gd_3Ga_9Ge single crystals reveal no anisotropy effects associated with the crystal field, in accord with *S*-ground state of Gd ions.

Acknowledgments

Financial support from the Department of Energy (Grant # DE-FG02-99ER45793) is gratefully acknowledged. This work made use of the SEM facilities of the Center for Advanced Microscopy at Michigan State University.

Supporting Information Further details of the crystal structure investigations may be obtained from the

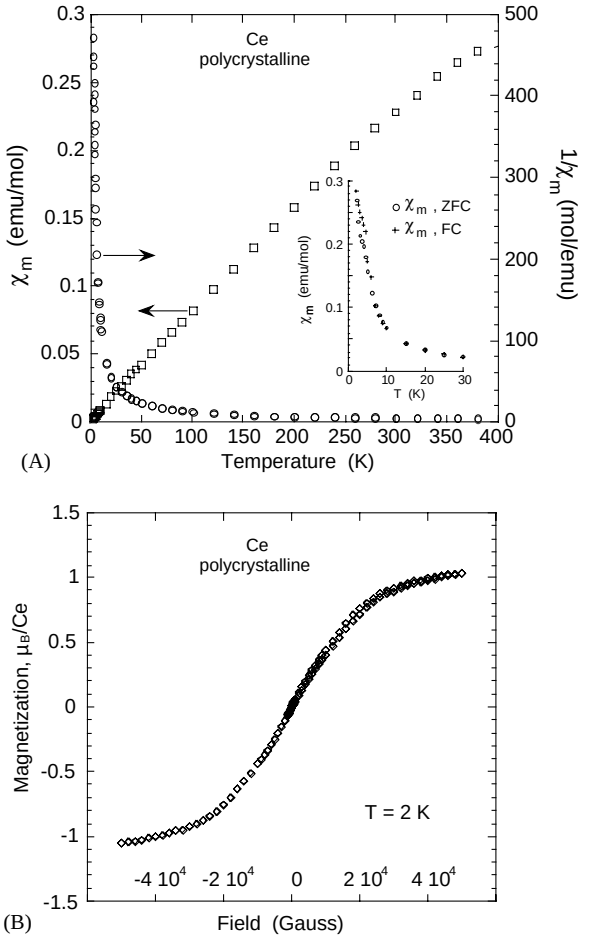

Fig. 11. Magnetization data for a polycrystalline sample of Ce_3Ga_9Ge. (A) Temperature dependence of molar magnetic susceptibility and inverse susceptibility; Inset: low-temperature region of magnetic susceptibility; (B) The magnetization in fields up to ± 5 T.

Fachinformationszentrum Karlsruhe, D-76344 Eggenstein-Leopoldshafen, Germany (fax: (+49) 7247-808-666; e-mail: crysdata@fiz-karlsruhe.de) on quoting numbers CSD-412648 and CSD-412649 for sub- and super-structures, respectively.

References

[1] X.Z. Chen, P. Small, S. Sportouch, M. Zhuravleva, P. Brazis, C.R. Kannewurf, M.G. Kanatzidis, Chem. Mater. 12 (2000) 2520.
[2] M.A. Zhuravleva, X.Z. Chen, X. Wang, A.J. Schultz, J. Ireland, C.R. Kannewurf, M.G. Kanatzidis, Chem. Mater. 14 (2002) 3066.
[3] M. Schlüter, W. Jeitschko, Inorg. Chem. 40 (2001) 6362.
[4] A. Lacerda, P.C. Canfield, W.P. Beyermann, M.F. Hundley, J.D. Thompson, G. Sparn, Z. Fisk, C. Burns, D. Barnhart, A.C. Lawson, G.H. Kwei, J. Goldstone, J. Alloys Compds. 181 (1992) 191.
[5] Ya.P. Yarmolyuk, Yu.N. Grin', I.V. Rozhdestvenskaya, O.A. Usov, A.M. Kuz'min, V.A. Bruskov, R.I. Gladyshevskii, Sov. Phys. Crystallogr. (translated from Kristallografyia) 27 (5) (1982) 599.
[6] Yu.N. Grin', Ya.P. Yarmolyuk, I.V. Rozhdestvenskaya, Sov. Phys. Crystallogr. (translated from Kristallografyia) 28 (4) (1983) 477.
[7] Yu.N. Grin', Ya.P. Yarmolyuk, V.E. Zavodnik, Sov. Phys. Crystallogr. (translated from Kristallografyia) 29 (2) (1984) 135.
[8] Yu.N. Grin', Ya.P. Yarmolyuk, O.A. Usov, A.M. Kuz'min, V.A. Bruskov, Sov. Phys. Crystallogr. (translated from Kristallografyia) 28 (6) (1983) 710.
[9] M. Schlüter, W. Jeitschko, Z. Anorg. Allg. Chem. 626 (2000) 2217.
[10] S.M. Kauzlarich (Ed.), Chemistry, Structure and Bonding of Zintl Phases and Ions, VCH Publishers, New York, 1996.
[11] CERIUS2, Version 1.6 Molecular Simulations Inc., Cambridge, England, 1994.
[12] SMART, Version 5; Siemens Analytical X-ray Systems, Inc., Madison, WI, 1998.
[13] SAINT, Version 4; Siemens Analytical X-ray Systems, Inc., Madison, WI, 1994–1996.
[14] B. Sieve, S. Sportouch, X.Z. Chen, J.A. Cowen, P. Brazis, C.R. Kannewurf, V. Papaefthymiou, M.G. Kanatzidis, Chem. Mater. 13 (2002) 273.
[15] B. Sieve, Doctoral Dissertation Thesis, Michigan State University, 2002.
[16] X.Z. Chen, B. Sieve, R. Henning, A.J. Schultz, P. Brazis, C.R. Kannewurf, J.A. Cowen, R. Crosby, M.G. Kanatzidis, Angew. Chem. Intl. Ed. Engl. 38 (1999) 693.
[17] B. Sieve, X.Z. Chen, R. Henning, P. Brazis, C.R. Kannevurf, J.A. Cowen, A.J. Schultz, M.G. Kanatzidis, J. Am. Chem. Soc. 29 (2001) 7040.
[18] M.A. Zhuravleva, R.J. Pcionek, X. Wang, A.J. Schultz, M.G. Kanatzidis, submitted for publication.
[19] L.M. Gelato, E. Parthé, J. Appl. Crystallogr. 20 (1987) 139.
[20] M.A. Zhuravleva, Doctoral Dissertation Thesis, Michigan State University, 2002 (Chapter VI).
[21] M.A. Zhuravleva, Doctoral Dissertation Thesis, Michigan State University, 2002 (Chapter VII).
[22] P. Zhuravleva, M.A. Kanatzidis. M.G., work in progress.
[23] L. Pauling, The Nature of Chemical Bond and the Structures of Molecules and Solids, Cornell University Press, Ithaca, NY, 1960.
[24] B.D. Sharma, J. Donohue, Z. Kristallogr. 117 (1962) 293.
[25] R.I. Gladishevskii, K. Cenuzal, H.D. Flack, E. Parthé, Acta Crystallogr. B 49 (1993) 468.
[26] V. Thiede, B. Fehrmann, W. Jeitschko, Z. Anorg. Allg. Chem. 625 (1999) 1417.
[27] M.A. Zhuravleva, K.K. Rangan, M. Lane, P. Brazis, C.R. Kannewurf, M.G. Kanatzidis, J. Alloys Compds. 316 (2001) 137.
[28] R. Pöttgen, G. Kotzuba, E. Görlich, K. Latka, J. Solid State Chem. 141 (1998) 352.
[29] A. Szytula, J. Leciejewicz, Handbook of Crystal Structures and Magntic Properties of Rare-Earth Intermetallics, CRC Press, Boca Raton, FL, 1994 (Chapter 4).
[30] J.J. Rhyne, in: R.J. Elliot (Ed.), Magnetic Properties of Rare Earth Metals, Plenum Press, London and New York, 1972.
[31] D. Niepmann, R. Pöttgen, B. Künnen, G. Kotzuba, C. Rosenhahn, B. Mosel, Chem. Mater. 11 (1999) 1597.
[32] R. Pöttgen, H. Borrmann, R.K. Kremer, J. Magn. Magn. Mater. 152 (1996) 196.
[33] C.D.W. Jones, R.A. Gordon, F.J. DiSalvo, R. Pöttgen, R.K. Kremer, J. Alloys Compds. 260 (1997) 50.
[34] T. Sugawara, H. Eguchi, J. Phys. Soc. Jpn. 21 (1966) 725.
[35] D.T. Adroja, B.D. Rainford, Physica B 194/196 (1994) 363; B.D. Rainford, D.T. Adroja, Physica B 194/196 (1994) 365.